Food and Bioproducts Processing 137 (2023) 145–154

Available online at www.sciencedirect.com

Food and Bioproducts Processing

journal homepage: www.elsevier.com/locate/fbp

The cleanability of laser etched surfaces with repeated fouling using *Staphylococcus aureus* and milk

Kathryn Whitehead[a,*], *Lisa I. Pilkington*[b], *Anthony J. Slate*[c], *Fabien Saubade*[a], *Mohsin Amin*[a], *Adrian Lutey*[d], *Laura Gemini*[e], *Rainer Kling*[e], *Luca Romoli*[d,*]

[a] *Microbiology at Interfaces, Manchester Metropolitan University, Chester St, Manchester, UK*
[b] *School of Chemical Sciences, University of Auckland, Auckland 1010, New Zealand*
[c] *Department of Life Sciences, University of Bath, Claverton Down, Bath BA2 7AY, UK*
[d] *Department of Engineering and Architecture, University of Parma, Parco Area delle Scienze 181/A, Parma 43124, Italy*
[e] *ALPhANOV, Institut d'Optique d'Aquitaine, Rue François Mitterand, Talence 33400, France*

ARTICLE INFO

Article history:
Received 28 June 2022
Received in revised form
2 November 2022
Accepted 16 November 2022
Available online 25 November 2022

Keywords:
Patterned
Laser etching
Surface topography
Milk Fouling
Bacteria
Cleaning

ABSTRACT

Biofouling is a serious problem in the food industry, and one way to control biofouling is using topographically patterned surfaces. This *in vitro* study used a laser surface texturing process to produce six differently patterned topographies which were analysed for their topography and wettability with repeated fouling and cleaning. The surfaces were spray-inoculated with *Staphylococcus aureus* suspended in either sterile distilled water or whole milk, then spray-cleaned using a chlorinated, alkaline cleaner. The surfaces were cleaned up to 20 times and analysed for changes in their surface properties and biofouling. Analysis of Variance was used to assess the effect of the main factors and two-way interactions. Principal component analysis was used to discern underlying relationships. There were no significant differences (T-Tests) in the overall level of biofouling between the different rippled sub-textures. The spiked surfaces showed no overall increase in biofouling and the number of cleans but were predominantly influenced by the texture sub-type. The less regular spiked surfaces within the medium range showed the lowest levels of biofouling, even with repeated cleaning. This study demonstrated that the use of such surfaces in *in vitro* studies may reduce biofouling, but particular attention needs to be given to the surface design.

1. Introduction

Due to the complexity of food processing facilities, large surface areas and residual organic matter, food production facilities provide an ideal environment for bacterial attachment and biofilm formation (Yuan et al. 2020). The accumulation of microorganisms and/or organic material can result in biofouling of surfaces and the potential

* Corresponding authors.
E-mail addresses: K.a.whitehead@mmu.ac.uk (K. Whitehead), luca.romoli@unipr.it (L. Romoli).

https://doi.org/10.1016/j.fbp.2022.11.007

contamination of food products and hence biofouling is a significant problem throughout the food industry (Whitehead et al. 2015; Yemmireddy and Hung, 2017). This can result in changes to the food quality resulting in food spoilage, which is defined as a 'change in the quality of food that renders it undesirable and unfit for consumption, either by humans or animals, due to spoilage indicators such as objectionable odour and changes in texture and appearance' (Lianou et al. 2016). This can ultimately also result in risks to the safety of the food. The sfaety of the food refers to that which is not injurious to health and is fit for human consumption (EU, 2002; Feliciano et al. 2020). Microbial contamination of food products has a significant economic burden on consumers (e.g absence from work), food companies and traders (Bintsis, 2017).

Throughout the food industry, the level of microorganisms present is continually monitored as a verification of the cleaning process and this is often determined as the total viable count (Møretrø and Langsrud, 2017). *Staphylococcus aureus* is a foodborne pathogen of particular importance (Miao et al. 2019), especially throughout the meat and dairy industries (Gutiérrez et al., 2012). The food-handler is believed to be the most likely cause of *S. aureus* contamination, however, other studies have suggested that dairy cows suffering from mastitis may be an alternative source of *S. aureus* (Gallina et al. 2013; Johler et al. 2013; Kümmel et al., 2016). The production of Staphylococcal endotoxins, which can cause nausea, stomach cramps and diarrhoea, can withstand pasteurisation techniques and are resistant towards human gastrointestinal proteases (Balaban and Rasooly, 2000). There have been considerable foodborne outbreaks due to *S. aureus* reported, between 1988 and 2008 and up to 87% of vomiting cases in the USA alone were due to *S. aureus* contamination (Xu et al. 2008; Bennett et al. 2013; Liu et al. 2018).

One approach to resist microbial biofouling is the alteration of surface properties of food production surfaces. By changing the properties of a surface topographically, chemically or physicochemically, it may be that new surface designs can be achieved that reduce biofouling on a surface. An understanding of such parameters that reduce surface biofouling may then be used to design more robust surfaces that could eventually be used in industrial applications to reduce the risk of surface contamination. One example is the utilisation of modified surfaces (Moerman, 2014; Zouaghi et al. 2019). Such materials have specific surface properties, for example the lotus leaf is superhydrophobic and demonstrates self-cleaning attributes in specific conditions, whilst other surfaces such as shark skin, can reduce drag during movement through water (Koch and Barthlott, 2009). Zouaghi et al. (2017) produced a novel biomimetic, slippery, liquid-infused stainless steel which was evaluated under industrial dairy pasteurisation conditions. Stainless steel surfaces (316 L 2B) were textured *via* femtosecond laser ablation to generate cauliflower like micro- and nanotopographies providing a dual-scale surface morphology. These surfaces were then chemically modified with a fluorosilane prior to being impregnated with a perfluorinated oil and it was found that a twenty minute rinsing step with water was sufficient to remove fouled dairy contaminants (artificial milk) (Zouaghi et al. 2017). Other surface modifications include those that have specific topographies (Varin et al. 2013; Tsibidis et al. 2015), wettabilities and/or (Sun et al. 2018) chemical functionalities which have been tested to determine if such surfaces can reduce the propensity for biofouling. However, there are a number of difficulties, in testing such surfaces, since it is known that in an industrial setting the bacteria will be in organic material, the chemical used in the cleaning process can alter the surface and bacterial properties, and the scaling up of the surfaces used in *in vitro* studies may be difficult to the complexity or robustness of the surfaces, or the production methods. However, experimental assays provide valuable insights into understanding how surface properties influence surface biofouling.

The aim of the current study was to develop and characterise novel, topographically patterned, laser etched surfaces and evaluate cleanability of the surfaces following repeated fouling with both milk and *S. aureus*, to demonstrate the feasibility of such surfaces being utilised within the dairy industry.

2. Material and methods

2.1. *Surface production*

Three coupons (5 cm × 5 cm) of stainless steel 304 L, each containing nine areas (1 cm × 1 cm), were provided. Six different surfaces were provided from AlphaNov (France) and included Infrared (IR) Nanopillars, IR Ripples, Ultraviolet (UV) Ripples, Small (S) Spikes, Medium (M) Spikes and Large (L) Spikes. All surface texturing processes were conducted by utilising a Tangerine Laser system (Amplitude System) with a central wavelength of 1030 nm and pulse duration of ~320 fs. The system can deliver up to 20 W of average power with a maximum repetition rate of 2 MHz. For processes carried out in UV regime, a module for generation of third harmonics (343 nm) was placed in front of the laser source to convert the main IR wavelength. The laser beam was firstly shaped through a specific telescope and then directed through a galvanometric scanning head which moved the laser beam on the sample surface at speeds up to 5 m/s. The beam was finally focused on the sample by a f-theta lens with focal length of 100 mm to obtain a focused beam spot diameter of about 25 μm for IR wavelength and 15 μm for UV wavelength. The scanning geometry employed for all the processes was a succession of parallel lines separated by a specific inter-line hatch distance. Each line was composed by overlapping pulses with a distance between pulses defined by the ratio between the scanning speed and the repetition rate. During all tests, an aspiration system was employed to suction the ablation dust produced during the laser texturing. Table 1 summarises the process parameters employed for the texturing of each surface (Bechert et al. 2000).

2.2. *Scanning electron microscopy (SEM)*

Scanning electron microscope (SEM) images were acquired by using a high resolution SEM VEGA3 system from Tescan. Acquisition was carried out using a secondary electron detector in high vacuum mode with an accelerating voltage of 30 V. No cleaning procedure was used after the laser processing prior to the SEM analyses.

2.3. *Surface inoculation*

To assess bacterial attachment on the six types of surfaces provided, *Staphylococcus aureus* strain NCIMB 11832/NCTC 4163 was selected to be sprayed on the surfaces. Prior to surface inoculation, overnight suspensions were prepared by

Table 1 – Process parameters employed for the laser texturing of stainless steel surfaces.

Process parameters	IR Ripples	IR Nanopillars	Spikes S, M, L	UV Ripples
Repetition rate (kHz)	1000	250	1000	200
Average power (W)	1.5	1	8	0.16
Number of scans	1	1	20	1
Scanning speed (m/s)	1	1.5	2	0.2
Polarization state	Linear	Azimuthal	Linear	Linear
Hatch distance (μm)	5	3	S: 2; M: 5; L: 8	5

using 5 mL of tryptone soya broth (TSB) inoculated with a single bacterial colony. The strain was incubated at 37 °C overnight, with agitation for 24 h. The bacterial suspensions were centrifuged thrice at 1721 *g* for 10 min at room temperature. After each centrifugation, the supernatant was discarded, and the pellets were suspended in 5 mL of sterile distilled water to wash the cells. The cell suspension was adjusted to an optical density (OD) of 0.99 ± 0.02 (*ca.* 8.87 ± 0.16 Log_{10} colony forming unit per mL) (CFU/mL) at 600 nm. Each coupon was used for one condition of inoculation: i) inoculation with sterile distilled water (W; Control), ii) inoculation with *S. aureus* in sterile distilled water (SaW), and iii) inoculation with *S. aureus* in whole milk (SaM). Whole milk was purchased at a local market, and used within two days after opening and was refrigerated until used. To prepare the suspensions of *S. aureus* in water and milk, 10 mL of either sterile distilled water or milk were inoculated with 20 μL of the suspension of OD 0.99. The concentration of *S. aureus* at the start of the experiments was determined to be 6.26 ± 0.10 and 6.31 ± 0.13 log_{10} CFU/mL, for *S. aureus* in sterile distilled water and *S. aureus* in whole milk respectively. For the inoculation, each coupon was fixed to a metallic plate previously sterilised with ethanol 70%, using double-sided adhesive tape. The metallic plate was attached to the back of a class II cabinet, so that the coupons were parallel to wall of the cabinet. The selected solutions and suspensions (sterile distilled water, *S. aureus* in sterile distilled water, or *S. aureus* in whole milk) were sprayed on the surfaces using an air propellant, for 3 s from a distance of 10 cm. The solutions and suspensions were sprayed onto the coupons using a compressed gas paint sprayer with a 0.5 mm nozzle size (Spraycraft Universal Air Propellant, Shesto, UK) inside a class II laminar flow cabinet (Faster, Italy). This corresponded to a volume of liquid spray of 0.3 mL which equated to 5.77 log_{10} CFU/mL. After each spray, the surfaces were dried in a class II cabinet, under sterile flowing air for one hour.

2.4. Cleaning assays

After each spray assay (inoculation of the surfaces), each surface was fixed again on a metallic plate, as for the inoculations. 0th clean refers to the surfaces before inoculation. A detergent, Chlorfoam (Holchem Laboratories, UK) which consisted of between 1% and 5% Sodium hypochlorite (content expressed as % available chlorine in solution) and 1% – 5% sodium laryl sulphonate was used to clean the surfaces. Chlorfoam 1.5% v/v was sprayed three times on each surface, with a one second interval between each spray. This corresponded to a total of 3.3 mL of detergent sprayed on each surface. The detergent was left to act for one minute on each surface. Each surface was then rinsed by spraying sterile distilled water for five seconds (0.5 mL). The surfaces were dried under sterile air flow in a class II cabinet for one hour. The inoculation followed by cleaning assay was repeated up to 20 times for each surface.

2.5. Optical profilometry

The control surfaces and the surfaces after 1, 5, 10, 15, and 20 cleaning assays were analysed *via* optical profilometry. Optical profilometry images were taken as previously described (Skovager et al. 2013). To take the images, a MicroXAM (phase shift) surface mapping microscope (ADE corporation, XYZ model 4400 mL system) with an AD phase shift controller (Omniscan, UK) was used. For each area, at least three images were taken before the first cleaning assay, and after the 1st, 5th, 10th, 15th, and 20th cleaning assays. In addition, from each image, three different roughness parameters were taken, S_a (average roughness), S_q (root mean square roughness; equivalent to the standard deviation of the heights), and S_{pv} (average peak to valley roughness) (n = 3).

2.6. Water contact angles (WCA) measurements

To assess the impact of the different treatments on the wettability of the surfaces, water contact angles were measured. The measurements were performed with HPLC grade water (BDH, UK), using a sessile drop Goniometer (Kruss, France). Five separate droplets were taken on five separate coupons from the same batch at different locations across the surfaces. For each droplet, the left and right contact angles were recorded, using the tangent method I, and the values were averaged.

2.7. Visualisation of Biofouling

The coverage of organic material and cells on the surfaces was analysed by epifluorescence directly after the optical profilometry and water contact angle measurements. Each surface analysed was covered with 2 mL of 0.03% w/v acridine orange (Sigma, UK) which had been dissolved in 2% v/v glacial acetic acid (Sigma, UK) for 2 min (under dark conditions). The surfaces were rinsed with 10 mL of sterile distilled water (SDW) and left in a class II cabinet air flow to dry under sterile air conditions. The surfaces were immediately analysed with an epifluorescence microscope (Nikon Eclipse E600, Surrey, UK), equipped with an F-View II black and white digital camera (Soft Imaging System Ltd, supplied by Olympus, UK) and a Cell F image analysis package.

2.8. Statistical analysis

Statistical analysis of the data was carried out using paired student Ttests using two-tailed distribution with two

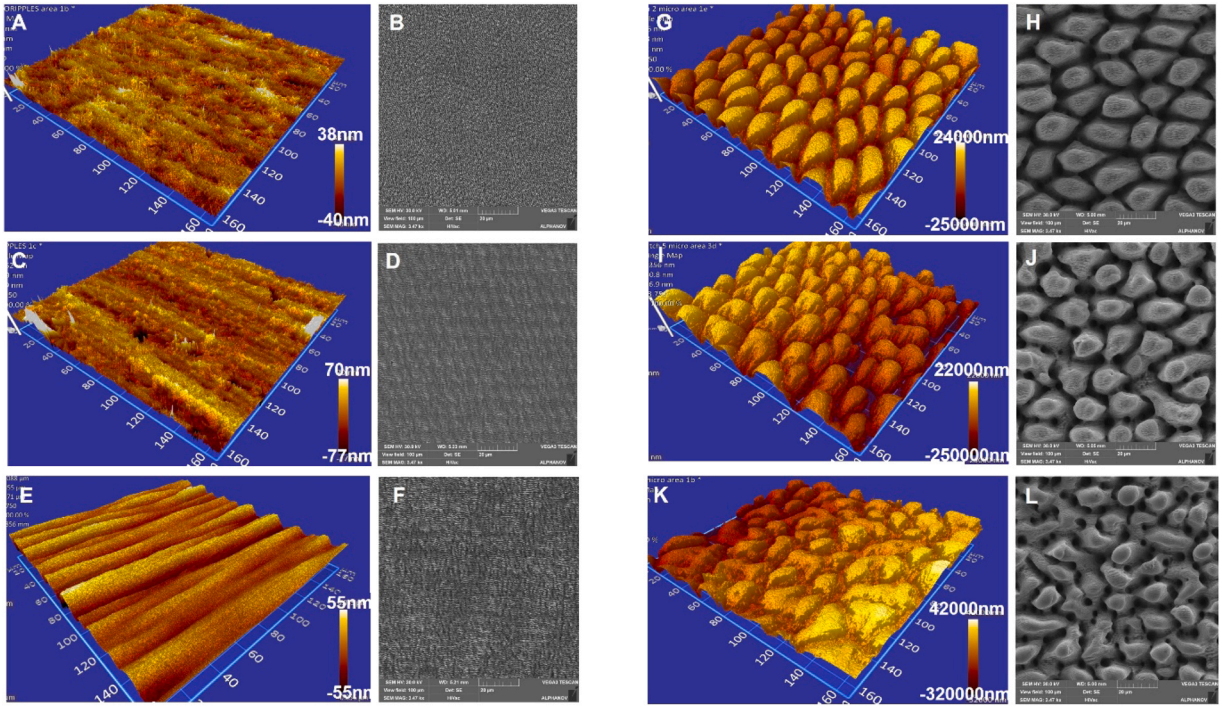

Fig. 1 – Optical profilometry (a-f) and scanning electron microscopy (Scale bar 20 µm) (g-l) images of the stainless steel surfaces with defined features. a/b) IR Nanopillars, c/d) IR Ripples e/f) UV Ripple g/h) Spikes S, 1/j) Spikes M and k/l) Spikes L surfaces.

sampled equal variance whereby $p < 0.05$ was considered significant.

2.9. *Multivariate analysis of variance (ANOVA) and principal component analysis (PCA)*

Statistical analyses were carried out using R. Multivariate analysis of variance (ANOVA) and multiple-pairwise comparison t-tests (with Benjamini and Hochberg *p*-value adjustment) were conducted using the aov and pairwise.t.test functions as part of the stats package (Team, 2013). Principal component analysis (PCA) was performed using the prcomp function as part of the stats package, by singular value decomposition of the centered and scaled data matrix (Team, 2013). Results of this analysis were visualized using the factoextra package (version 1.0.5) and ggplot2 (Wickham, 2016). Exploratory analysis graphs and additional plots were constructed using the various functions available in the ggplot2 and ggraph packages.

3. Results and discussion

The surfaces were produced and fully characterised and tested for their propensity to resist biofouling by bacteria, or bacteria and milk.

3.1. *Surface Morphology*

The surface structures were divided into two groups, rippled and spiked surfaces. Following texturing of the rippled surfaces, it was demonstrated using optical profilometry, that although all the surfaces had striated features, the IR Nanopillars surface (Fig. 1a) demonstrated the most irregular surface features that overlaid the striations, whilst the UV rippled surface demonstrated the clearest striations on the surface (Fig. 1e). Scanning electron microscopy (SEM) was conducted to confirm the topographies of the laser textured surfaces. IR (Fig. 1d) and UV (Fig. 1f) ripples topographies presented the classic periodic pattern of laser-induced periodic surface structures (LIPSS) generated by linearly polarised light with a periodicity between successive ripples slightly lower than the respective laser wavelength and direction perpendicular to the orientation of the laser polarization. IR Nanopillars (Fig. 1b) presented a rhomboidal print with average dimension of about 1 µm and were generated as a geometrical overlapping of different ripple directions which were connected to the use of azimuthally polarized light. More information on this particular process can be found (Lutey et al. 2018). Finally, peaks were observed after laser texturing at higher values of cumulative energy absorbed by the irradiated surface. The size and depth of these pillar-like structures increased as the hatch distance between the successive lines decreased, due to the hydrodynamic motions of the laser-irradiated material (Tsibidis et al. 2015). IR ripples (Fig. 1c/d) covered the pillars forming a nanometric/micrometric hierarchical structure.

The optical profilometry of the spiked surfaces demonstrated that the Spikes S surface had regularly shaped, defined surface pillar shaped features, with rounded heads (Fig. 1g/h). The Spikes M features were less regular in shape and distribution (Fig. 1i/j), whilst the Spikes L surfaces demonstrated the most heterogeneous shaped pillars and distribution of pillars (Fig. 1k/l).

3.2. *Surface roughness*

The surface roughness values were determined using S_a (the arithmetic average height parameter), S_q (root mean square; the standard deviation of the z height values) and S_{pv} (average peak-to-valley roughness) measurements (Verran and Whitehead, 2006; McClements et al. 2021). The surface

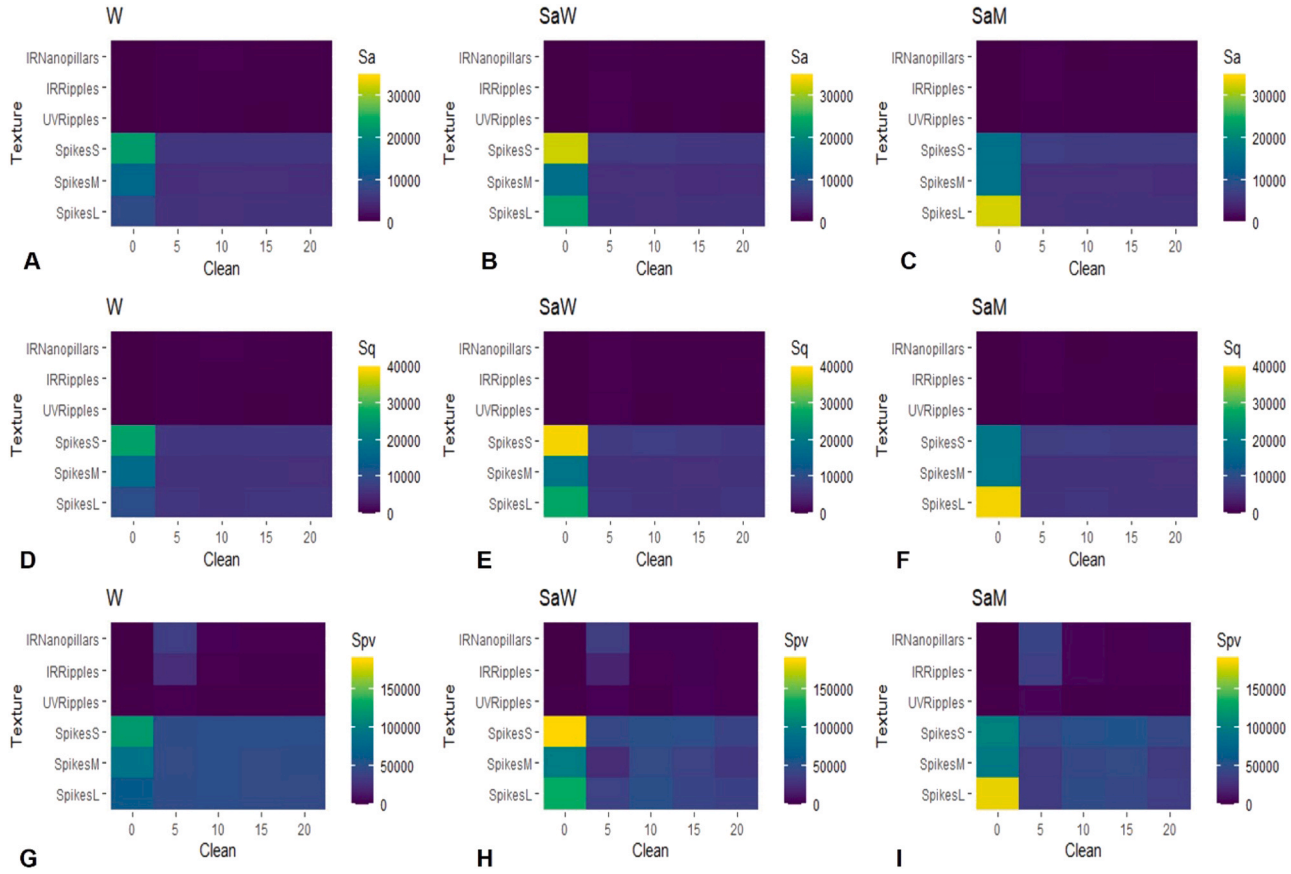

Fig. 2 – Heatmaps demonstrating the *Sa* (a-c), *Sq* (d-f) and *Spv* (g-i) of the six surfaces (UV Ripples, IR Ripples, IR Nanopillars, Spikes L, Spikes M and Spikes S) after the 0th, 5th, 10th, 15th and 20th cleaning cycle, with either water (W) (a, d and g), *S. aureus* and water (SaW) (b, e and h) or *S. aureus* and milk (SaM) (c, f and i). Darker cells = lower values.

roughness metrics, S_a, S_q and S_{pv} described below, are shown in the Supplementary Information in Figs. 1, 2 and 3.

3.2.1. S_a values

All the laser-treated surfaces rippled surfaces demonstrated S_a values between 11 nm and 75 nm prior to experimentation (0 clean, Supplementary information S1). Following the 5th clean, biofouling on all the surfaces was significantly reduced compared to the surfaces before cleaning. From the 10th clean onwards the amount of biofouling across all three surfaces was reduced, and from the 15th clean onwards the UV rippled surfaces demonstrated the least fouling for both *S. aureus* in sterile distilled water (188 nm) and *S. aureus* in whole milk (123 nm). For the spiked surfaces, all the cleaned surfaces demonstrated a significant reduction in their S_a values compared to the uncleaned surface (Supplementary information S1). There was no significant difference in the S_a values for the spiked surfaces when cleaned with *S. aureus* in water or in milk at the 5th, 10th, 15th and 20th cleans.

3.2.2. S_q values

Prior to the cleaning assays, the S_q values of the rippled surfaces were significantly lower, ranging between 18 nm and 42 nm, than the surface S_q values following cleaning (Supplementary Figure 2). The trends observed in the S_a values, described above, were similar to those observed for the S_q values. On all the rippled surfaces following fouling and cleaning, the largest S_q value was observed after the 5th clean. It was then observed that in general, there was a marked and significant decrease in S_q from the 5th to the 10th clean and the UV Rippled surface demonstrated the lowest S_q values following repeated fouling and cleaning with *S. aureus* in sterile distilled water and *S. aureus* in whole milk. All the spikes surfaces demonstrated significantly greater S_q values before cleaning was carried out (range 1056–3874 nm). Following cleaning, all the S_q values significantly reduced for the 5th, 10th, 15th or 20th cleans on all the surfaces regardless of the foulant. The Spikes M surface demonstrated the lowest topographies in S. aureus in whole milk (5664–5849 nm).

3.2.3. S_{pv} values

For the rippled surfaces, the control surfaces demonstrated low S_{pv} values (226–5633 nm) (Supplementary Fig. S3). Significantly higher S_{pv} values were observed at the 5th clean, but with subsequent cleaning, S_{pv} values decreased and after 20 cleans the UV Rippled surface demonstrated the lowest S_{pv} value. Analysis of the spiked surfaces demonstrated that all the surfaces demonstrated greater S_{pv} values pre-cleaning. At each clean level there was no significant difference in the S_{pv} values but Overall, the S_{pv} values were lowest on the Spikes M surfaces.

These results were consolidated using heatmaps (Fig. 2), and it was clearly demonstrated that the UV rippled surface, IR rippled surface and IR Nanopillars surfaces demonstrated lower S_a, S_p and S_{pv} values than the spike surfaces (dark navy in the heatmaps corresponding to low values). Furthermore, in the case of the spike surfaces, fouling with *S. aureus* in

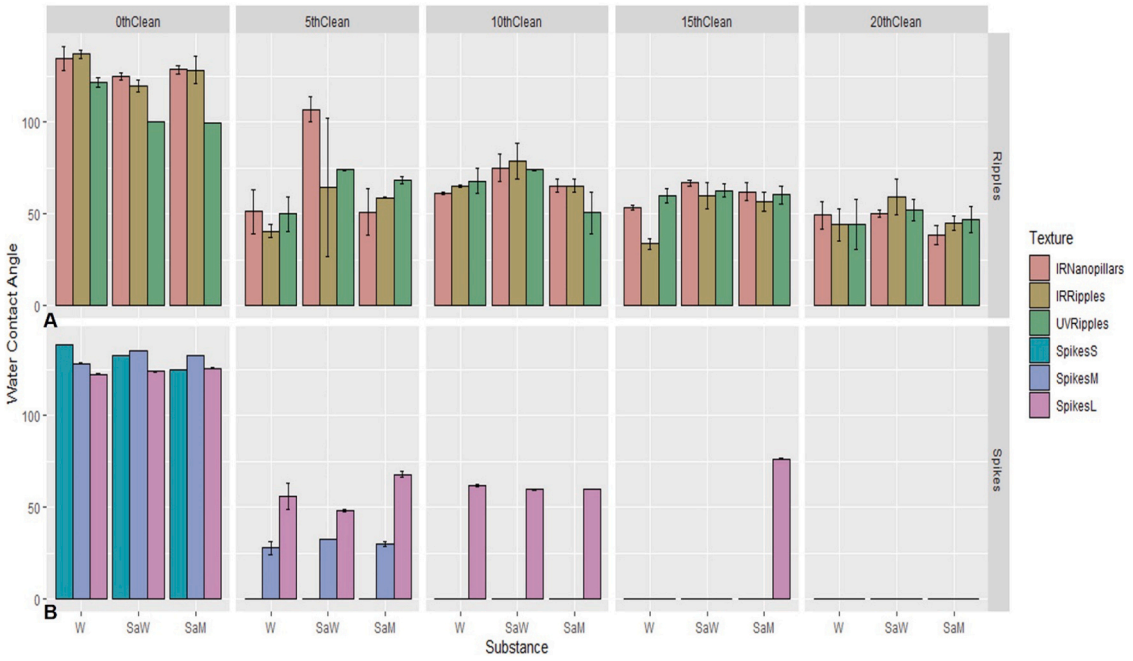

Fig. 3 – Water contact angles (WCA) of the surfaces following fouling and cleaning of surfaces in water (W) *S. aureus* in water (SaW) or *S. aureus* in milk (SaM) on the IR Nanopillars, IR Ripples and UV Ripple surfaces and Spikes S, Spikes M and Spikes L surfaces.

either water or milk resulted in increased S_a, S_p and S_{pv} values during the early stages of the cleaning procedure (light yellow in the heatmaps corresponding to high values), however, as the number of cleaning cycles increase, the S_a, S_p and S_{pv} values decreased. Hence, the use of S_a, S_p and S_{pv} values in this work demonstrated the varied differences on the surfaces following repeated biofouling for the rippled surfaces, and less pronounced differences in biofouling on the spiked surfaces. Laser treatment production of hierarchical structured surfaces can produce a wide range of topographical shapes and sizes, especially in microbiological terms. For example, when picosecond laser treatment was applied to stainless steel, the S_a, S_q and S_{pv} values ranged between 0.02 µm -1.16 µm, 0.02 µm – 1.30 µm and 0.82 µm – 9.84 µm (Rajab et al. 2018) which was comparable to those used in this study. An effect of surface topography on reducing biofouling has previously been shown where it was found that super-hydrophobic surfaces demonstrated a significant (nearly 50% decrease of the average microbe attachment area ratio) anti-biofouling effect as compared with a bare stainless steel plate; in addition it was shown that micro-grooved super-hydrophobic surfaces with more abundant hierarchical micro-nano structures showed better anti-biofouling performance than micro-pit, super-hydrophobic surfaces (Sun et al. 2018).

3.3. *Surface wettability*

Before the cleaning assays, the water contact angles (WCAs) of the rippled surfaces were indicative of all the surfaces being non-wettable (134.6°, 136.9° and 121.5° for the IR Nanopillars, IR ripples and UV Ripples, respectively) (Fig. 3a). Following cleaning and re-fouling with *S. aureus* and water, the surfaces became more wettable (range: IR Nanopillars range 38° - 108°; IR Ripples 59° - 79 °; UV Ripples 52° - 74°). Following re-fouling with a milk and *S. aureus* solution, the surfaces generally became even more wettable, in the range of; IR Nanopillars 65° - 38°, IR Ripples 45° - 65° and UV Ripples 47° - 68°. The water contact angles revealed no significant difference with increased cleans.

The spiked surfaces were non-wettable prior to cleaning (138.6 °, 128.4 ° and 122.5 ° for the Spike S, Spike M and Spike L respectively) (Fig. 3b). However, following cleaning, regardless of the solution or suspension used, the surfaces became so wettable that a water contact angle dispersed quickly and it could not be recorded. Work by others using a model foulant fluid also found an increase in surface wettability following fouling studies, and it was suggested that this was due to a thin layer of hydrophilic protein remaining on the surface from the previous cleaning cycle (Zouaghi et al. 2019). In our work, it may be that the differences following cleaning with water were an effect of residual detergent which may have had an effect of the spreading of the water across the different topographies, however, this phenomenon requires further investigation. Previous studies have shown that laser treatment production of hierarchical structured stainless steel demonstrated that the wettability of the surfaces ranged between 99.5 ° - 160 ° but no single physicochemical value was found to be attributed to all the surfaces that retained the greatest bacterial numbers (Rajab et al. 2018). Li et al. (2015) fabricated bio-mimic superhydrophobic surfaces with contact angles of 160° on polymer surfaces using nanoimprinting lithography techniques and reported that these surfaces were self-cleaning since *E. coli* adhesion was reduced by 60%. However, these assays did not include milk fouling or repetitive cleaning assays. Although many surfaces begin with hydrophobic or superhydrophobic properties, once fouled and cleaned, in agreement with this work, the surfaces may become more hydrophilic possibly due to residual organic material or cleaning fluid (Wilson-Nieuwenhuis et al. 2022). However, hydrophilic surfaces have also been shown to reduce biofouling. The biofouling propensity and cleaning effectiveness were evaluated for polyamide thin-film composite membranes that were surface

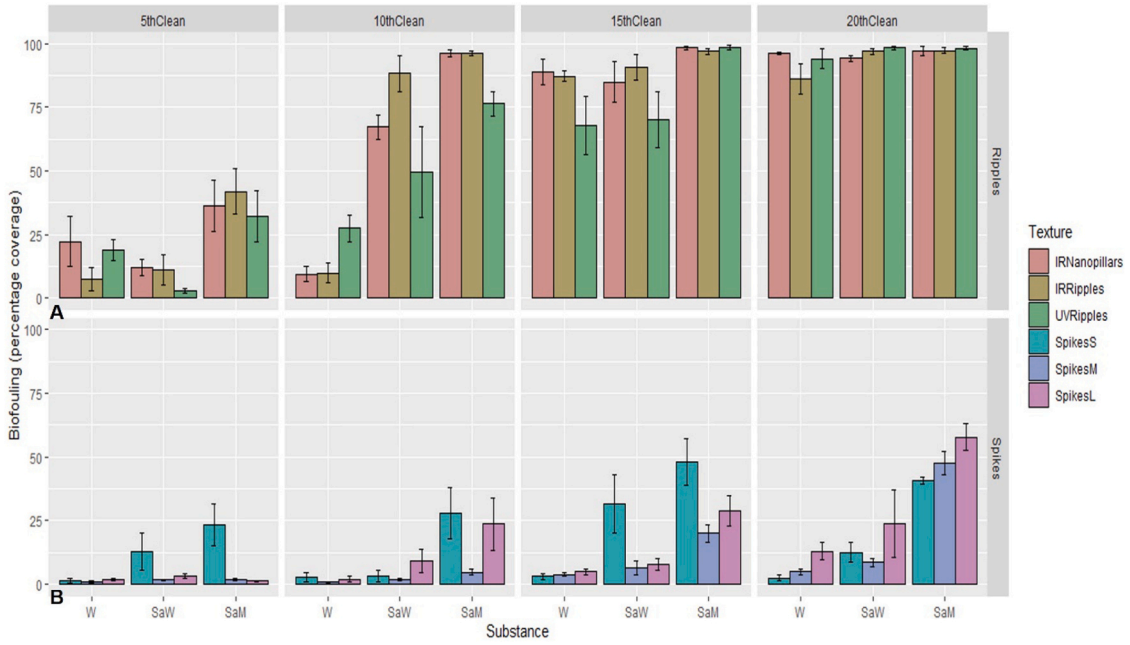

Fig. 4 – Percentage coverage of organic materials and cells remaining on the surfaces after 5, 10, 15 and 20 cleaning assays on a) control, IR Nanopillars, IR Ripples and UV Ripples and b) control, Spikes S, Spikes M and Spikes L inoculated with either surfaces in water (W) *S. aureus* in water (SaW) or *S. aureus* in milk (SaM).

nano-structured with terminally anchored hydrophilic polymer chains and the results suggested that biofouling resistance and cleaning effectiveness of membranes could be enhanced *via* hydrophilic brush layers (Varin et al. 2013). What does seem clear is that in order to fully understand bacterial:surface interactions and potentially develop anti-adhesive (or antimicrobial) alternatives, surfaces should be tested in conditions that represent their intended environment.

3.4. *Cleanability of the surfaces*

All the rippled surfaces became more significantly fouled with increased cleans, including those just carried out in water (Fig. 4a). Following refouling and cleaning with sterile distilled water, *S. aureus* in sterile distilled water and *S. aureus* in whole milk, after 10 cleans the UV Rippled surface demonstrated the lowest amount of biofouling, but by 20 cleans there was no significant difference in the surfaces. Following cleaning and refouling of the spiked surfaces, the surfaces cleaned in the presence of a water solution resulted in the least fouling. For the *S. aureus* in sterile distilled water surfaces, biofouling was low with only 8.6% coverage by 20 cleans. When refouled with *S. aureus* in milk, 40% fouling was observed at 20 cleans. Following repeated fouling with *S. aureus* in water, after 20 cleans, the Spikes M surface demonstrated low fouling (8.6%) but when fouled with *S. aureus* and milk demonstrated 47% fouling by 20 cleans. The Spikes L surfaces demonstrated that following cleaning with water, the greatest percentage coverage was obtained at 20 cleans (23.8%). When refouled with *S. aureus* and milk, after 20 cleans the largest percentage coverage of the three surfaces was demonstrated (57.8%). In agreement wit these findings, work by Zouaghi et al. (2019) also determined that a difference in the fouling performance of surfaces, was mainly driven by the differences in surface morphology.

3.5. *Multivariate analysis of variance (ANOVA)*

ANOVAs were carried out to formally assess the effect of each of the main factors (Substance: water, *S. aureus* in water, *S. aureus* in milk; texture type: rippled or spiked; texture subtype: IR Nanopillars, IR ripples, UV Ripples, Spikes S, Spikes M and Spikes L; Clean: number of cleans being 0, 5, 10, 15, 20) on the WCA as well as appropriate two-way interactions (substance and type of texture, substance and number of cleans, and texture sub-type and number of cleans). Results of the analysis indicated that most factors analysed were significant (p values < 0.05). Exploring each of the levels of the main factors, whilst holding all else constant, the WCA of the surface was higher for the surfaces that underwent refouling with *S. aureus* in water / *S. aureus* in milk, compared to water alone and the rippled surfaces had a WCA significantly higher than spiked surfaces. Within the rippled surfaces, there was no significant difference between the rippled texture subtypes, IR Nanopillars, IR ripples and UV Ripples, matching the observation of similar trends in WCA for these surfaces. In contrast, Spikes L was shown to have significantly different surface wettability profiles compared to both the Spikes S and Spikes M surfaces. In general, it was shown that biofouling was highest for repeated fouling with *S. aureus* in milk, then *S. aureus* in water, then water. It was also shown that rippled surfaces had higher levels of biofouling than spiked surfaces. There were no significant differences in the overall level of biofouling between the ripple sub-textures, although there was some evidence that Spikes S had generally higher levels than the Spikes M surfaces. It was seen that the number of cleans had a significant and notable effect on the biofouling of the surfaces.

3.6. *Principal component analysis (PCA)*

In addition to analysis of each of the attributes measured, separately, principal component analysis (PCA) was used to

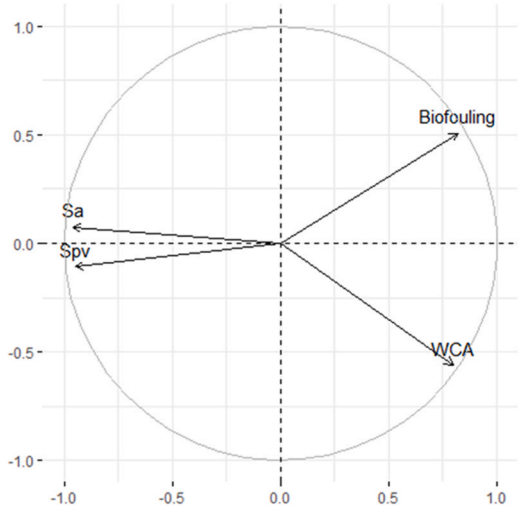

Fig. 5 – PCA loadings plot for the first two principal components (PC1 on the x-axis and PC2 on the y-axis), visualising the relationships between each of the measures analysed in this study.

Fig. 6 – PCA biplot visualising relationships between the surface roughness measures (S_a, S_q and S_{pv} values), WCA and biofouling percentage for each of the surfaces and cleaning conditions. The 95% ellipsoids represent clusters based on surface texture type as the key variable with the following colours for each: spiked (blue) and rippled (red).

uncover underlying trends on how the surface roughness metrics, water contact angle (*i.e.*, surface wettability) and surface biofouling related to each other, and to determine how the different surfaces compared when taking into account all of these measures, simultaneously. This was an important tool to use since following the accumulation of data that was complex with large variation due to the parameters tested, thus PCA was used to confirm the findings of the information content. Principal component 1 (PC1, accounting for ~78% of the total variation in the data) was mostly dictated by the surface roughness measurements but was also moderately contributed to, by the water contact angle and biofouling percentage (Fig. 5). PC2 (~15%) was mainly influenced by the water contact angle and biofouling percentage, although in opposite directions, indicative that these two variables are somewhat positively correlated (same direction with respect to PC1) but this relationship is only weak-to-moderate in strength. Most of the variation in the data was captured in the first two principal components (78% and 15%) with PC3 representing < 5% (scree plot not

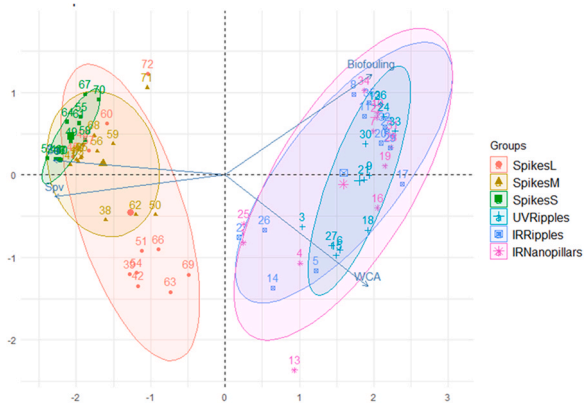

Fig. 7 – PCA biplot visualising relationships between the surface roughness measures (S_a, S_q and S_{pv} values), WCA and biofouling percentage for each of the surfaces and cleaning conditions. The colouring of the points and 95% ellipsoids represent the sample surface texture sub-type.

shown). Therefore, the PCA discussed herein was informed by analysis of PC1 and PC2, with these accounting for ~93% of the variability in the data.

The direction of the vectors in the PCA showed that the surface roughness measurements were strongly positively correlated to each other, particularly the S_a and S_q values which showed an extremely high degree of correlation. Two measurements were shown to be negatively correlated to each other, *i.e.*, increasing surface roughness was indicative of decreasing WCA and biofouling percentage. This was in agreement to previous work that has shown that using picosecond etched surfaces, the lowest S_a, S_q and S_{pv} demonstrated the highest number of bacteria retained (Rajab et al. 2018). Specifically designed surface structures on Ti6Al4V surfaces by picosecond laser surface texturing demonstrated that the trimodally dimensioned surface roughness, with a blunt conical macro-topography was effective at reducing bacterial fouling following attachment, adhesion and retention assays using *E. coli* (Rajab et al. 2017). However, no conditioning film was used in the assays, nor was any cleaning protocols.

When colouring each of the samples in the biplot by their texture (rippled or spiked) it was apparent that this was a critical feature in defining and characterising the surface, as demonstrated by the clear groupings and separated texture-defined clusters (Fig. 6, 95% confidence ellipsoids shown). Interpreting this result and the PCA, it was demonstrated that the spiked surfaces (blue) exhibited higher surface roughness measurements and had lower water contact angles and biofouling levels than the rippled surfaces (red).

With regard to the surface characteristic profile, it was apparent that the surface texture sub-type was not particularly influential for the rippled surfaces, as indicated by the overlapping 95% ellipsoids for the IR Nanopillars, IR Ripples and UV Ripples (Fig. 7). In contrast, the properties of the different sub-types of spiked surfaces did notably differ, which was evidenced by the altering position and orientation of the ellipsoids for Spikes S (green), Spikes M (yellow) and Spikes L (red) surfaces. The Spikes S surfaces had less variability in their characteristics, followed by the Spikes M, and the Spikes L surfaces were the most varied, as indicated by the size of the ellipsoids. The Spikes S surfaces generally had lower water contact angles, biofouling and higher surface roughness, than the other spiked sub-types. Given that

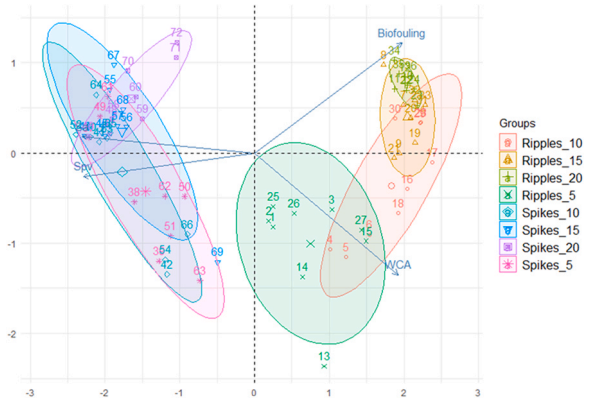

Fig. 8 – PCA biplot visualising relationships between the surface roughness measures (S_a, S_q and S_{pv} values), WCA and biofouling percentage for each of the surfaces and cleaning conditions. The colouring of the points and 95% ellipsoids represent the sample surface texture and number of cleans. The value in the key refers to the number of cleans of the surfaces.

there were no clear differences in the range of spiked surfaces in terms of wettability or surface roughness, it might be suggested that the surface properties of the Spikes M surface, along with the features of the surface topography enabled this surface to be the least fouled during cleaning under the conditions used in this study. Such results highlight the need for careful consideration of surface design when producing surfaces to reduce fouling in specific environments.

Whilst the texture sub-type was shown to be a discerning feature in determining the measured characteristics (S_a, S_q, S_{pv} values, WCA, biofouling), it was observed that the number of cleans was particularly decisive and influential for the properties of the rippled surfaces (Fig. 8). The metrics measured for the rippled surfaces changed with number of cleans, particularly the WCA and biofouling, although it can be seen that the surface roughness values for 5 cleans (light green) were higher than for 10, 15 and 20 cleans. With an increasing number of cleans from 5 (light green), to 10 (red), to 15 (yellow) to 20 (green), the water contact angle of the rippled surface decreased, and biofouling increased. In contrast, it can be surmised that the number of cleans was not particularly inducive to a change in surface properties for the spiked surfaces, which as stated above was instead predominantly influenced by the texture sub-type.

4. Conclusions

The spiked surfaces had much rougher surface features than the rippled featured surfaces. The rippled surfaces were all fouled by 20 cleans and regardless of surface type or clean, had higher levels of biofouling in milk than the spiked surfaces and demonstrated an increase in biofouling as the number of cleaning cycles increased. There were no significant differences in the overall level of biofouling between the different rippled sub-textures. The number of cleans particularly affected the properties of the rippled surfaces, predominantly the wettability and biofouling. Surface texture sub-type did not influence biofouling of the rippled surfaces. The spiked surfaces showed no overall increase in biofouling and the number of cleans was not inducive to a change in surface properties. However, biofouling of the surfaces with spike topographies were predominantly influenced by the texture sub-type. In particular, Spikes M showed the lowest levels of biofouling, even with repeated cleaning. This study demonstrated that the use of such surfaces in *in vitro* studies may reduce biofouling, but particular attention needs to be given to the surface design.

Funding

This research did not receive any specific grant from funding agencies in the public, commercial, or not-for-profit sectors.

Declaration of Competing Interest

The authors declare that they have no known competing financial interests or personal relationships that could have appeared to influence the work reported in this paper.

Appendix A. Supporting information

Supplementary data associated with this article can be found in the online version at doi:10.1016/j.fbp.2022.11.007.

References

Balaban, N., Rasooly, A., 2000. Staphylococcal enterotoxins. Int. J. Food Microbiol. 61, 1–10.

Bechert, D., Bruse, M., Hage, W., Meyer, R., 2000. Fluid mechanics of biological surfaces and their technological application. Naturwissenschaften 87, 157–171.

Bennett, S.D., Walsh, K.A., Gould, L.H., 2013. Foodborne disease outbreaks caused by Bacillus cereus, Clostridium perfringens, and Staphylococcus aureus—United States, 1998–2008. Clin. Infect. Dis. 57, 425–433.

Bintsis, T., 2017. Foodborne pathogens. AIMS Microbiol. 3, 529.

EU 2002 European Parliament and Council. Regulation (EC) No 178/2002 of 28 January 2002 Laying Down the General Principles and Requirements of Food Law, Establishing the European Food Safety Authority and Laying Down Procedures in Matters of Food Safety; European Parliament and Council of the European Union: Brussels, Belgium, Volume L31, 1–24.

Feliciano, R.J., Boué, G., Membré, J.-M., 2020. Overview of the potential impacts of climate change on the microbial safety of the dairy industry. Foods 9, 1794.

Gallina, S., Bianchi, D.M., Bellio, A., Nogarol, C., Macori, G., Zaccaria, T., Biorci, F., Carraro, E., Decastelli, L., 2013. Staphylococcal poisoning foodborne outbreak: epidemiological investigation and strain genotyping. J. Food Prot. 76, 2093–2098.

Gutiérrez, D., Delgado, S., Vazquez-Sanchez, D., Martinez, B., Cabo, M.L., Rodriguez, A., Herrera, J.J., Garcia, P., 2012. Incidence of *Staphylococcus aureus* and analysis of associated bacterial communities on food industry surfaces. Appl. Environ. Microbiol. 78, 8547–8554.

Johler, S., Tichaczek-Dischinger, P.S., Rau, J., Sihto, H.M., Lehner, A., Adam, M., Stephan, R., 2013. Outbreak of Staphylococcal food poisoning due to SEA-producing Staphylococcus aureus. Foodborne Pathog. Dis. 10, 777–781.

Koch, K., Barthlott, W., 2009. Superhydrophobic and superhydrophilic plant surfaces: an inspiration for biomimetic materials. Philos. Trans. R. Soc. A: Math. Phys. Eng. Sci. 367, 1487–1509.

Kümmel, J., Stessl, B., Gonano, M., Walcher, G., Bereuter, O., Fricker, M., Grunert, T., Wagner, M., Ehling-Schulz, M., 2016. *Staphylococcus aureus* entrance into the dairy chain: tracking S. aureus from dairy cow to cheese. Front. Microbiol. 7, 1603.

Li, Y., John, J., Kolewe, K.W., Schiffman, J.D., Carter, K.R., 2015. Scaling up nature—large area flexible biomimetic surfaces. ACS Appl. Mater. Interfaces 7, 23439.

Lianou, A., Panagou, E.Z., Nychas, G.J.E., 2016. Microbiological spoilage of foods and beverages. In: Subramaniam, P. (Ed.), The Stability and Shelf Life of Food, Second ed. Woodhead Publishing, Duxford, UK, pp. 3–42.

Liu, J., Deng, Y., Li, L., Li, B., Li, Y., Zhou, S., Shirtliff, M.E., Xu, Z., Peters, B.M., 2018. Discovery and control of culturable and viable but non-culturable cells of a distinctive *Lactobacillus harbinensis* strain from spoiled beer. Sci. Rep. 8, 1–10.

Lutey, A.H.A., Gemini, L., Romoli, L., Lazzini, G., Fuso, F., Faucon, M., Kling, R., 2018. Towards laser-textured antibacterial surfaces. Sci. Rep. 8, 10112.

McClements, J., Gomes, L.C., Spall, J., Saubade, F., Akhidime, D., Peeters, M., Mergulhão, F.J., Whitehead, K.A., 2021. Celebrating the centenary in polymer science: drawing inspiration from nature to develop anti-fouling coatings. Pure Appl. Chem. 93 (10), 1097–1108.

Miao, J., Soteyome, T., Peters, B.M., Li, Y., Chen, H., Su, J., Li, L., Li, B., Xu, Z., Shirtliff, M.E., Harro, J.M., 2019. Biofilm formation of *Staphylococcus aureus* under food heat processing conditions: first report on CML production within biofilm. Sci. Rep. 9, 1–9.

Moerman, F., 2014. Antimicrobial materials, coatings and biomimetic surfaces with modified microtopography to control microbial fouling of product contact surfaces within food processing equipment: legislation, requirements, effectiveness and challenges. J. Hyg. Eng. Des. 7, 8–29.

Møretrø, T., Langsrud, S., 2017. Residential bacteria on surfaces in the food industry and their implications for food safety and quality. Compr. Rev. Food Sci. Food Saf. 16, 1022–1041.

Rajab, F.H., Liauw, C.M., Benson, P.S., Li, L., Whitehead, K.A., 2017. Production of hybrid macro/micro/nano surface structures on Ti6Al4V surfaces by picosecond laser surface texturing and their antifouling characteristics. Colloids Surf. B: Biointerfaces 160, 688–696.

Rajab, F.H., Liauw, C.M., Benson, P.S., Li, L., Whitehead, K.A., 2018. Picosecond laser treatment production of hierarchical structured stainless steel to reduce bacterial fouling. Food Bioprod. Process. 109, 29–40.

Skovager, A., Whitehead, K.A., Wickens, D., Verran, J., Ingmer, H., Arneborg, N., 2013. A comparative study of fine polished stainless steel, TiN and TiN/Ag surfaces: adhesion and attachment strength of Listeria monocytogenes as well as antilisterial effect. Colloids Surf. B: Biointerfaces 109, 190–196.

Sun, K., Yang, H., Xue, W., He, A., Zhu, D., Liu, W., Adeyemi, K., Cao, Y., 2018. Anti-biofouling superhydrophobic surface fabricated by picosecond laser texturing of stainless steel. Appl. Surf. Sci. 436, 263–267.

Team, R.C. (Vienna, Austria, 2013).

Tsibidis, G.D., Fotakis, C., Stratakis, E., 2015. From ripples to spikes: a hydrodynamical mechanism to interpret femtosecond laser-induced self-assembled structures. Phys. Rev. B 92, 041405.

Varin, K.J., Lin, N.H., Cohen, Y., 2013. Biofouling and cleaning effectiveness of surface nanostructured reverse osmosis membranes. J. Membr. Sci. 446, 472–481.

Verran, J., Whitehead, K.A., 2006. Assessment of organic material and microbial components on hygienic surfaces. Food Bioprod. Process. 84, 260–264.

Whitehead, K.A., Benson, P., Verran, J., 2015. Developing application and detection methods for Listeria monocytogenes and fish extract on open surfaces in order to optimize cleaning protocols. Food Bioprod. Process. 93, 224–233.

Wickham, H., 2016. ggplot2: Elegant Graphics for Data Analysis. Springer.

Wilson-Nieuwenhuis, J., Dempsey-Hibbert, N., Liauw. C.M., Whitehead, K.A. 2022. The effect of human blood plasma conditioning films on platelet transfusion bag surface properties. Applied Science, Accepted.

Xu, Z., Li, L., Alam, M.J., Zhang, L., Yamasaki, S., Shi, L., 2008. First confirmation of integron-bearing methicillin-resistant *Staphylococcus aureus*. Curr. Microbiol. 57, 264–268.

Yemmireddy, V.K., Hung, Y.C., 2017. Using photocatalyst metal oxides as antimicrobial surface coatings to ensure food safety—opportunities and challenges. Compr. Rev. Food Sci. Food Saf. 16, 617–631.

Yuan, L., Hansen, M.F., Røder, H.L., Wang, N., Burmølle, M., He, G., 2020. Mixed-species biofilms in the food industry: current knowledge and novel control strategies. Crit. Rev. Food Sci. Nutr. 60, 2277–2293.

Zouaghi, S., Six, T., Bellayer, S., Moradi, S., Hatzikiriakos, S.G., Dargent, T., Thomy, V., Dargent, T., Andre, C., Delaplace, G., Jimenez, M., 2017. Antifouling biomimetic liquid-infused stainless steel: application to dairy industrial processing. ACS Appl. Mater. Interfaces 9, 26565–26573.

Zouaghi, S., Bellayer, S., Thomy, V., Dargent, T., Dargent, T., Andre, C., Delaplace, G., Jimenez, M., 2019. Biomimetic surface modifications of stainless steel targeting dairy fouling mitigation and bacterial adhesion. Food Bioprod. Process. 113, 32–38.